PERGAMON

Chemical Engineering Science 55 (2000) 5763–5771

Chemical Engineering Science

Structural transitions in methane + ethane gas hydrates — Part I: upper transition point and applications

S. Subramanian[a], A. L. Ballard[a], R. A. Kini[a], S. F. Dec[b], E. D. Sloan Jr.[a,*]

[a]*Center for Hydrate Research, Colorado School of Mines, Golden, CO 80401-1887, USA*
[b]*Department of Chemistry and Geochemistry, Colorado School of Mines, Golden, CO 80401-1887, USA*

Received 14 February 2000; accepted 24 May 2000

Abstract

Although methane and ethane form sI hydrates by themselves, the binary gas mixtures of these components form sII hydrates at certain compositions. In our earlier work, it was reported that the structure of methane + ethane hydrates changes from sI to sII over a methane vapor composition range (y_{CH_4}) of 0.72–0.75. In this work, Raman spectroscopic measurements on $CH_4 + C_2H_6$ system suggest that the hydrate structure reverts from sII to sI over a y_{CH_4} range of 0.992 ($\pm$ 0.005)–0.994 ($\pm$ 0.007). ^{13}C NMR measurements on this system suggest that the methane hydrate composition increases by at least 0.2 mole fraction at the lower structural transition point. Predictions suggest that the hydrate structure above the incipient hydrate formation conditions may be different than that at the incipient conditions. The practical applications of these structural transitions in the $CH_4 + C_2H_6$ hydrates are discussed.

Keywords: Hydrate structure; Methane; Ethane; Model; Raman; NMR

1. Introduction and background

Natural gas hydrates are crystalline inclusion compounds with a well-defined structure that consists of a cage network of water molecules with hydrocarbon guests trapped inside the cages. The three known natural gas hydrate structures — sI, sII and sH — have unique combinations of various cavity types. The size and shape of the guest molecules determine the hydrate structure (Sloan, 1998).

Typical natural gases encountered in oil and gas production contain methane above 85 mol%, with ethane and higher paraffins comprising the balance (Katz et al., 1959). Since methane and ethane are two major components of natural gases, hydrates formed from these gases are of practical significance. The hydrate phase equilibria of these pure components and their binary mixtures have been measured over a number of years (Deaton & Frost, 1946; Holder & Grigoriou, 1980; Holder & Hand, 1982; McLeod & Campbell, 1961). Kinetic studies of hydrate formation from pure methane and ethane as well as their binary mixtures can also be found in the literature (Englezos, Kalogerakis, Dholabhai & Bishnoi, 1987a,b; Skovborg & Rasmussen, 1994). However, measurement of the hydrate structures was not done in these studies resulting in possible problems. For example, it may be difficult to combine the kinetics of pure methane and pure ethane sI hydrates if the gas mixtures form sII, a different hydrate structure with different kinetics.

Since methane and ethane are relatively small molecules, they each form sI hydrates (von Stackelberg & Jahns, 1954). However, it was shown in our previous work that the binary gas mixtures of methane and ethane form sII hydrates at certain compositions showing a structural transition from sI to sII over the range of 72.2–75 mol% methane at 274.2 K (Subramanian, Kini, Dec & Sloan, 2000). This composition range was referred to as the 'lower transition point'. Because pure methane, situated at one of the extremes of the composition range, forms sI hydrate, the structure of methane + ethane hydrates must revert from sII to sI with an increase in the methane composition above 75 mol%.

In this work, Raman spectroscopic measurements were used to obtain the vapor composition at which the hydrate structure changes from sII to sI. This composition

* Corresponding author. Tel.: +1-303-273-3723; fax: +1-303-273-3730.
E-mail address: esloan@gashydrate.mines.edu (E. D. Sloan Jr.).

0009-2509/00/$ - see front matter
PII: S0009-2509(00)00162-7

range is referred to as the 'upper transition point'. Also, ^{13}C NMR spectroscopy was used to obtain the guest composition of the hydrate phase on a water-free basis at various vapor compositions near the lower transition point.

The major significance of this work is to be able to use the spectroscopic data to obtain the best parameters for prediction of multicomponent mixtures. The measured lower structural transition point was used with a Gibbs energy minimization method to model the entire hydrate phase diagram of the methane + ethane + water system. This method was used to predict hydrate phase equilibria under excess water conditions at both transition points and intermediate compositions.

2. Experimental details

2.1. Apparatuses

Here we include only a brief overview of the Raman and NMR spectrometers. Further details can be found in Subramanian et al. (2000).

2.1.1. Raman spectrometer

A Renishaw Inc. MK III fiber-optic-based system equipped with a CCD detector was used in this work. A 514.53 nm Ar-ion laser providing 10 mW power at the sample was used for excitation. The spectral resolution was 4.5 cm^{-1}. The temperature and pressure measurements have a precision of $\pm$ 0.1 K and $\pm$ 0.014 MPa (2 psia), respectively. The representative Raman spectrum of a sample was obtained by averaging the spectra obtained from different points within the sample. The spectra were analyzed using GRAMS/32® software from Galactic Industries Corporation.

2.1.2. NMR spectrometer

A Chemagnetics CMX Infinity 400 NMR spectrometer was used in this study. Spectra were recorded at 253 K by placing samples within a 7.5 mm zirconia rotor loaded into a Chemagnetics variable temperature probe. All ^{13}C NMR spectra were obtained at a frequency of 100.6 MHz with proton decoupling during acquisition, magic angle spinning ($\sim$ 2.3 kHz) and single pulse excitation.

Radio frequency field strengths of 50–62.5 kHz corresponding to 4–5 μs ^{13}C $\pi/2$ pulses were used. Decoupling field strengths of 50–62.5 kHz were used. A relaxation delay of 150 s was used between the pulses in order to allow complete relaxation of the sample. The number of acquisitions varied from 100 to 300 depending on the amount of hydrate in the sample, which determines the signal intensity of the spectrum. The chemical shifts were referenced via sample substitution to the methyl resonance of hexamethylbenzene, which was assigned a chemical shift of 17.355 ppm. All chemical shifts are therefore reported relative to tetramethylsilane. The sample temperature was calibrated using methanol as the chemical shift thermometer (van Geet, 1970). The temperature measurements have a precision of $\pm$ 0.5 K.

3. Procedure

Research grade (99.92%) methane and C. P. grade (99%) ethane were acquired from General Air Company. Gas mixtures of methane and ethane were gravimetrically prepared in stainless steel cylinders. Mixtures were thermally agitated using an infra-red source. Because three out of four hydrate samples used for Raman studies were prepared from binary gas mixtures with methane compositions above 99 mol%, a 'double-dilution' method was adopted to prepare these high-methane mole fraction gas mixtures.

In this 'double-dilution' method, a starting gas mixture containing 89.7 mol% methane and 10.3 mol% ethane was prepared. Subsequent preparation of gas mixtures containing $>$ 99 mol% methane was achieved by diluting this mixture with a known amount of pure methane. The amount of methane required to be added was estimated via a calibration curve relating the increase of methane mass to the differential pressure of methane gas needed for this increase. A high-precision weighing balance was used to determine the final composition of these gas mixtures. The uncertainty in mixture composition was $\pm$ 0.1 mol%.

For Raman studies, the hydrate samples were prepared in a thick-walled Pyrex capillary cell from 0.02 ml of DI water and the desired gas mixture. To expedite hydrate formation, a magnetic wire was moved continuously in the sample using an external magnet. These samples were then conditioned at 274.2 K for a period of several days at pressures that were 2–3% higher than the experimentally determined L_w–H–V equilibrium conditions.

For NMR studies, a precision bore Pyrex glass tube with a small bulb at one end was used as the sample cell (Miyoshi, Takegoshi & Terao, 1997). The glass bulb was about three-fourths filled with finely powdered ice, formed from DI water, and pressurized with a gas or gas mixtures to about 3–4 MPa. The sample cell was conditioned at 273 K for 2–3 days and subsequently at temperatures above the ice point to facilitate an increase in the hydrate conversion. Further, the sample cell was evacuated by keeping the bulb immersed in liquid N_2 before a known amount of original gas was condensed in the bulb such that the final pressure in the sealed bulb was 2–3 MPa upon heating to 253 K. The glass bulb was then sealed off from the tube using a torch and used as the sample cell. These samples were conditioned at 253 K for a period of 1–8 months.

4. Experimental results and discussion

4.1. Raman studies

Four different $CH_4 + C_2H_6$ gas mixtures were used in this study to form hydrate samples. The methane mole fractions in these mixtures were 0.918, 0.991, 0.994, and 0.996. Fig. 1 shows the C–H region Raman spectra obtained from these $CH_4 + C_2H_6$ hydrate samples at 274.2 K and three-phase L_w–H–V equilibrium conditions. The average final vapor compositions in equilibrium with hydrates are shown beside the spectra. Each spectrum in this figure has contributions from both CH_4 and C_2H_6 Raman bands although C_2H_6 peaks in the upper two spectra are too weak to be distinguished because of the very low amounts of C_2H_6 in the hydrate phase.

In our previous work, it was shown that C_2H_6 resonance doublet Raman bands occur at 2891.2 and 2946.2 cm^{-1} in sI hydrates and at 2887.3 and 2942.3 cm^{-1} in sII hydrates (Subramanian et al., 2000). The v_1 totally symmetric C–H stretching of CH_4 in the small (5^{12}) and large ($5^{12}6^2$) cages of sI occurs at 2915.0 and 2904.8 cm^{-1}, respectively (Sum, Buruss & Sloan, 1997). Frequencies of 2913.7 and 2903.7 cm^{-1} were assigned to the v_1 symmetric stretching for CH_4 in the small (5^{12}) and large ($5^{12}6^4$) cages, respectively, of sII hydrates (Sum et al., 1997). In this work, the ethane resonance doublet was not used to determine the hydrate structure since the intensities of these peaks were too small.

Instead, the symmetric C–H stretching bands of CH_4 in the hydrate phase are used to infer structure type. It can be seen from Fig. 1 that the relative intensity of the CH_4 v_1 bands corresponding to large and small cavities in the hydrate, changes abruptly as the methane mole fraction in vapor (y_{CH_4}) increases from 0.992 ($\pm$ 0.005) to 0.994 ($\pm$ 0.007). This is based on the fact that there are twice as many small cages (5^{12}) as large cages ($5^{12}6^4$) in sII, and three times as many large cages ($5^{12}6^2$) as small cages (5^{12}) in sI.

This result clearly shows that the hydrate structure changes from sII to sI over a y_{CH_4} range of 0.992 ($\pm$ 0.005)–0.994 ($\pm$ 0.007). These vapor compositions were calculated using CH_4 and C_2H_6 band areas in the spectrum of the vapor in equilibrium with the hydrates. Band areas were used with a calibration curve generated for the high-methane mole fraction gas mixtures relating band areas to y_{CH_4}. A similar procedure was used to obtain the final vapor composition in our lower transition point study (Subramanian et al., 2000).

4.2. NMR studies

^{13}C NMR spectra were used to obtain the water-free guest composition of the hydrate phase at eight different vapor compositions. Hydrate structures in these samples

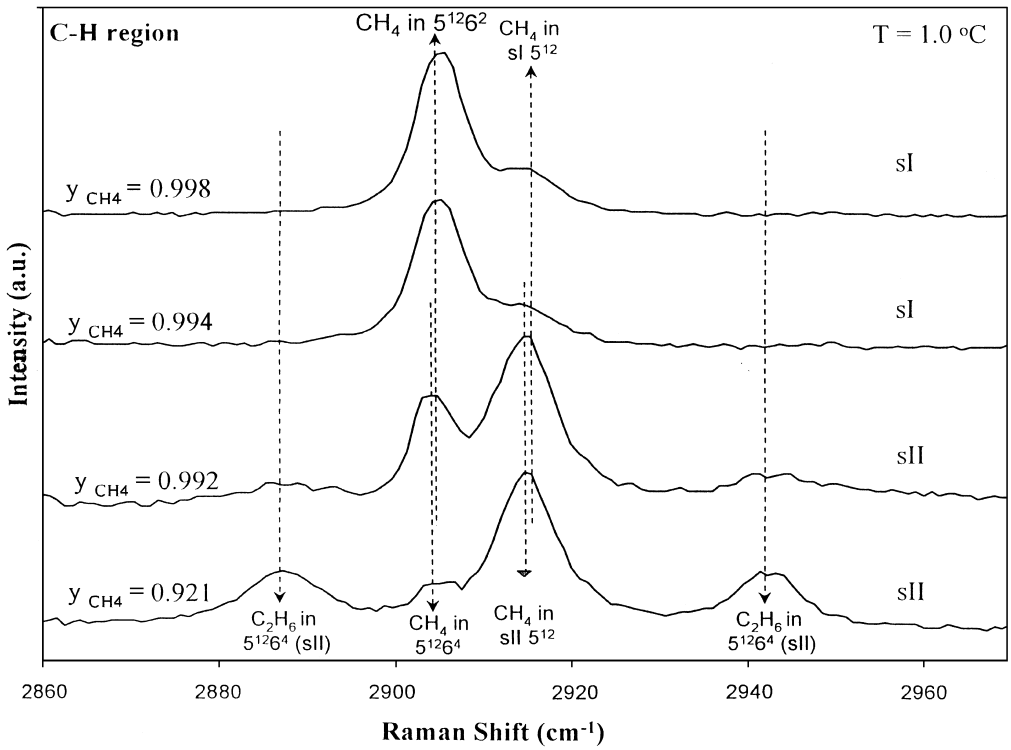

Fig. 1. Raman spectra of the C–H region for four different $CH_4 + C_2H_6$ hydrates obtained at 274.2 K and close to L_w–H–V equilibrium conditions. Contributions from both CH_4 and C_2H_6 can be seen in the spectra. Note the abrupt change in CH_4 peak intensities as vapor composition increases from $y_{CH_4} = 0.992$ to 0.994.

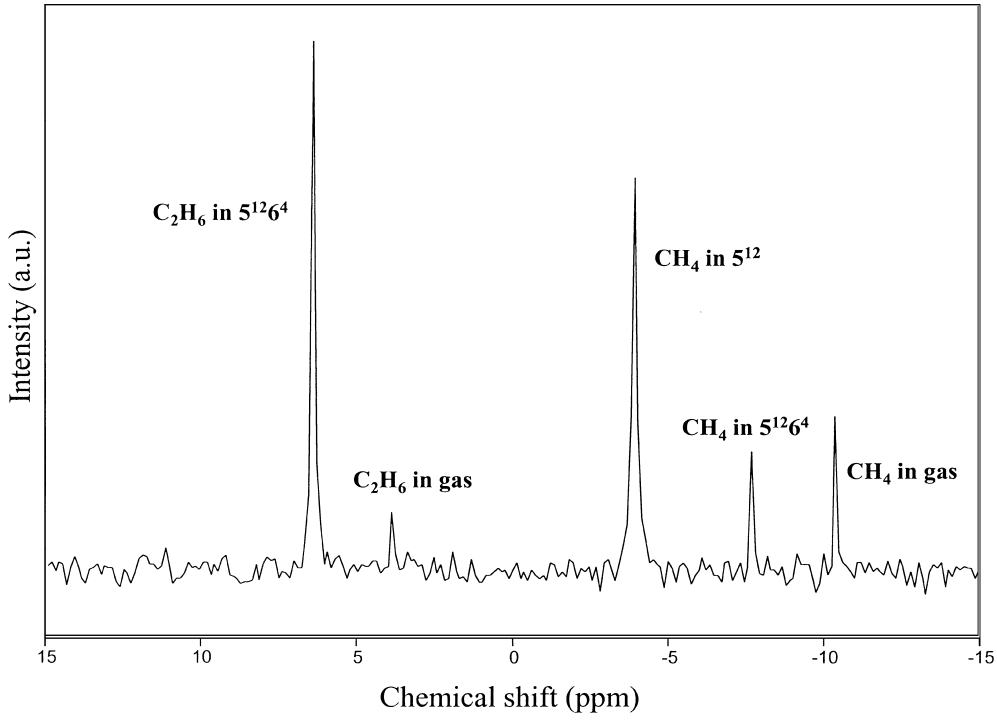

Fig. 2. ^{13}C NMR spectrum of $CH_4 + C_2H_6$ hydrate with $y_{CH_4} = 0.827$ at 253 K. Note that it has contributions from CH_4 and C_2H_6 in both the hydrate and the gas phases.

were identified based on chemical shift values of CH_4 and C_2H_6 in different cavities (Subramanian et al., 2000). Some of these samples had both sI and sII hydrates existing together. In such cases, the hydrate composition was obtained by taking into account all the CH_4 and C_2H_6 in the hydrate lattice, irrespective of its structure.

Fig. 2 shows the ^{13}C NMR spectrum for a $CH_4 + C_2H_6$ sII hydrate with $y_{CH_4} = 0.827$ at 253 K. This spectrum has resonance lines from C_2H_6 trapped in $5^{12}6^4$ cavities and in the gas phase as well as from CH_4 in 5^{12} and $5^{12}6^4$ cavities and the gas phase, as indicated. Such spectra were collected for all the samples but are not shown here. The peak intensities from ^{13}C NMR spectra were used to obtain the composition of both the hydrate and the gas phase in these samples.

The composition of the hydrate phase, z_{CH_4} can be calculated using

$$z_{CH_4} = \frac{A_{CH_4,large} + A_{CH_4,small}}{A_{CH_4,large} + A_{CH_4,small} + (A_{C_2H_6,large}/2)}. \quad (1)$$

$A_{CH_4,large}$, $A_{CH_4,small}$, and $A_{C_2H_6,large}$ correspond to the areas under the peaks for CH_4 in the small, large, and C_2H_6 in the large cages of either sI or sII or both, respectively. The ethane peak area is halved to account for two carbon atoms in an ethane molecule. Similarly, vapor phase composition (y_{CH_4}) can be calculated using

$$y_{CH_4} = \frac{A_{CH_4,gas}}{A_{CH_4,gas} + (A_{C_2H_6,gas}/2)}. \quad (2)$$

Fig. 3 shows a plot of z_{CH_4} against y_{CH_4} for the eight different $CH_4 + C_2H_6$ hydrate samples used in this study. It can be seen that there is a sudden increase in the hydrate composition by at least 0.2 methane mole fraction as vapor composition increases from $y_{CH_4} = 0.686$ to 0.784. This is due to a change in the hydrate structure. This observation is similar to the one reported in our earlier paper (Subramanian et al., 2000) based on the Raman results at 274.2 K. Note that the vapor compositions at 0.735 and 0.990 were estimated using Raman spectra as described in the previous section, because ^{13}C NMR peaks for the gas phase were too weak to derive any quantitative information. For similar reasons, the vapor composition at y_{CH_4} of 0.180 is assumed to be the same as feed gas composition.

It should be noted that both sI and sII coexist at compositions close to the lower and upper transition points. Here we present two possible reasons for this structural coexistence. According to Gibbs' phase rule, in a three-component (CH_4, C_2H_6, and water) and four-phase (vapor, sI, sII, and ice) system, there is only one degree of freedom, which means that these four phases can coexist at only one pressure at a given temperature. Because the pressures varied between our samples, it can be concluded that these samples are metastable in nature. On the other hand, if we assume that all ice is converted to hydrates, the additional degree of freedom can be used to vary the sample pressure. In this case, coexistence of sI and sII hydrates is thermodynamically possible.

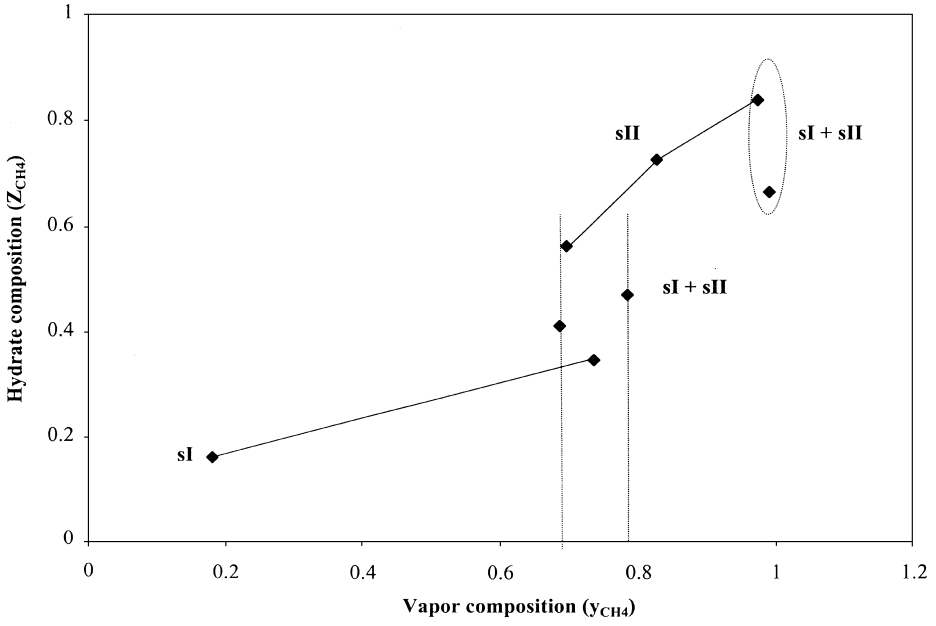

Fig. 3. Hydrate compositions (z_{CH_4}) obtained from ^{13}C NMR spectra of eight different samples are plotted as a function of equilibrium vapor compositions (y_{CH_4}). Note the sudden change in hydrate composition values over the y_{CH_4} range of 0.686–0.784, due to change in structure from sI to sII. The upper and lower compositions of this range are marked with vertical lines.

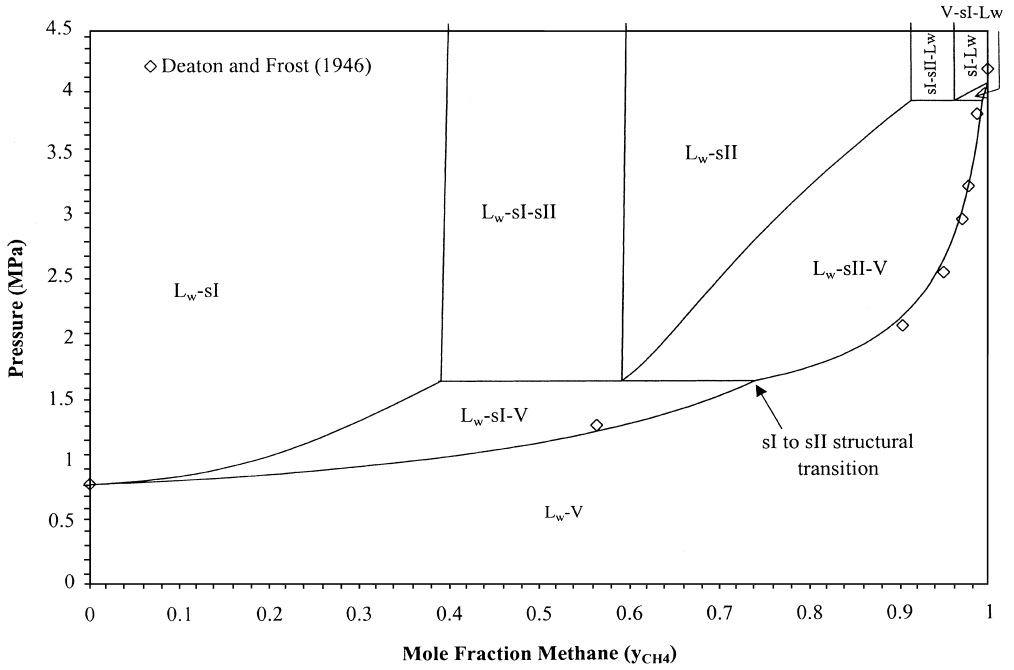

Fig. 4. The complete pressure versus composition phase diagram or methane + ethane + water system at 277.6 K. Note that the incipient hydrate equilibrium data by Deaton and Frost (1946), also plotted in the diagram, compare well with the model predictions. The lower and upper transition points were predicted to be at $y_{CH_4} = 0.74$ and 0.993, respectively.

Fig. 4 shows a predicted pressure–composition diagram for this system generated using the Gibbs energy minimization method (to be discussed in the next section). Structural coexistence can be seen in the region $0.4 < y_{CH_4} < 0.6$ and $P > 1.7$ MPa, where all the gas is predicted to be consumed to form both sI and sII hydrates. Nevertheless, experimental evidence to support either of the above arguments is awaited.

5. Modeling

5.1. Introduction

The model used to calculate phase equilibria for methane + ethane + water in this work is a multiple-phase Gibbs energy minimization method, based on the methodology of Bishnoi and co-workers (Gupta, 1990; Gupta, Bisnoi & Kalogerakis, 1991). In this work, the method is applied to map out the phase diagram of the methane + ethane + water system at and above incipient hydrate formation conditions.

This model is able to predict phase equilibria involving the hydrate structures — sI, sII, and sH, liquid water (L_w), liquid hydrocarbon (L_{hc}), and vapor (V). All fluid phases (V,L_w,L_{hc}) are described by the Soave–Redlich–Kwong equation of state while the solid hydrate phases are described by the theory of van der Waals and Platteeuw (1959). The Kihara spherical core potential is used to calculate the Langmuir constants. The Kihara parameters, σ and ε, were fit to incipient hydrate equilibrium data of pure components as well as the lower structural transition point obtained from Raman spectroscopy. The spectroscopic data were used to optimize the Kihara parameters of methane and ethane by forcing the model to predict the experimentally determined lower transition point at 274.2 K. The optimization procedure and the new set of Kihara parameters for CH_4 and C_2H_6 are presented in Ballard and Sloan (2000).

Previous hydrate prediction methods, such as the method developed by Parrish and Prausnitz (1972), are capable of calculating hydrate phase properties at incipient formation conditions. The method of Bishnoi and co-workers, however, can calculate hydrate phase properties at any temperature and pressure. Bishnoi, Gupta, Englezos and Kalogerakis (1989) have demonstrated this for natural gas systems using phase amount versus pressure diagrams. In this work, we have applied the method to the methane + ethane + water system to generate pressure versus composition and pressure versus temperature diagrams.

5.2. Results and discussion

Fig. 4 shows the complete pressure versus composition (P–x) phase space for methane + ethane + water at 277.6 K, generated using the above model. Hydrate equilibrium data at L_w–H–V equilibrium conditions by Deaton and Frost (1946) are also plotted to compare the model predictions with experimental data. The model predicts these incipient hydrate formation data well. At 277.6 K, the predictions show that the incipient hydrate structure changes from sI to sII at a $y_{CH_4} = 0.74$ with increasing methane concentration and the upper transition point from sII to sI is predicted to occur at approximately 99.3 mol% methane. It should be noted that predictions from the model guided the experimental Raman work at 274.2 K to determine the upper transition point at this temperature by suggesting that the transition occurs at high-methane mole fractions.

As the model predicts incipient hydrate formation data well, it can be extended to predict hydrate phase behavior at pressures above the incipient conditions. In the composition range of 0–74% methane, sI hydrates are predicted to form at the incipient conditions (Fig. 4). However, for initial compositions of about 40–60% CH_4, as the pressure is increased to about 1.7 MPa and above, sII is predicted to coexist with sI hydrates. A similar region is predicted in the composition range of about 90–95 mol% methane and pressures above 4 MPa. In the composition ranges of about 60–74 and 95–99.3 mol% methane, the hydrate structure at higher pressures is predicted to be different than that at incipient conditions.

A pressure versus temperature (P–T) section of the phase diagram for the water-free gas composition of $y_{CH_4} = 0.73$ is given in Fig. 5. It can be seen that sI hydrates are predicted to form initially in the temperature range of 277.5–277.7 K. However, with a minute increase in pressure (about 0.03 MPa) from the incipient conditions, sII hydrates are predicted to replace sI hydrates and persist at higher pressures. At 277.6 K temperature, as pressure is increased, sI hydrates are predicted to form at 1.61 MPa. With a further increase in pressure to 1.64 MPa, sI hydrates disappear and sII hydrates form.

The entire incipient hydrate equilibrium literature data set for the methane + ethane + water system is plotted in Fig. 6 in a natural logarithm of pressure versus temperature diagram. The sII stability envelope, which is the locus of lower and upper structural transition points, is shown within two intersecting dark lines in the diagram (dashed region). It can be seen that over 50% of the methane + ethane hydrate literature data are within the sII stability envelope, even though these mixtures were previously assumed to form sI hydrates at the incipient conditions.

6. Applications

Most natural gases in pipelines are predominantly methane up to about 85%, with ethane and propane as the other prominent components. While small amounts of propane normally cause sII hydrate formation, the upper transition point in the $CH_4 + C_2H_6$ system suggests that, even without propane or heavier components, sII hydrate is likely to predominate in pipeline situations. Even more importantly, the structural transition data can be used in generating better model parameters for methane and ethane, which in turn allow for more accurate predictions of hydrate forming conditions of natural gas systems (Ballard & Sloan, 2000).

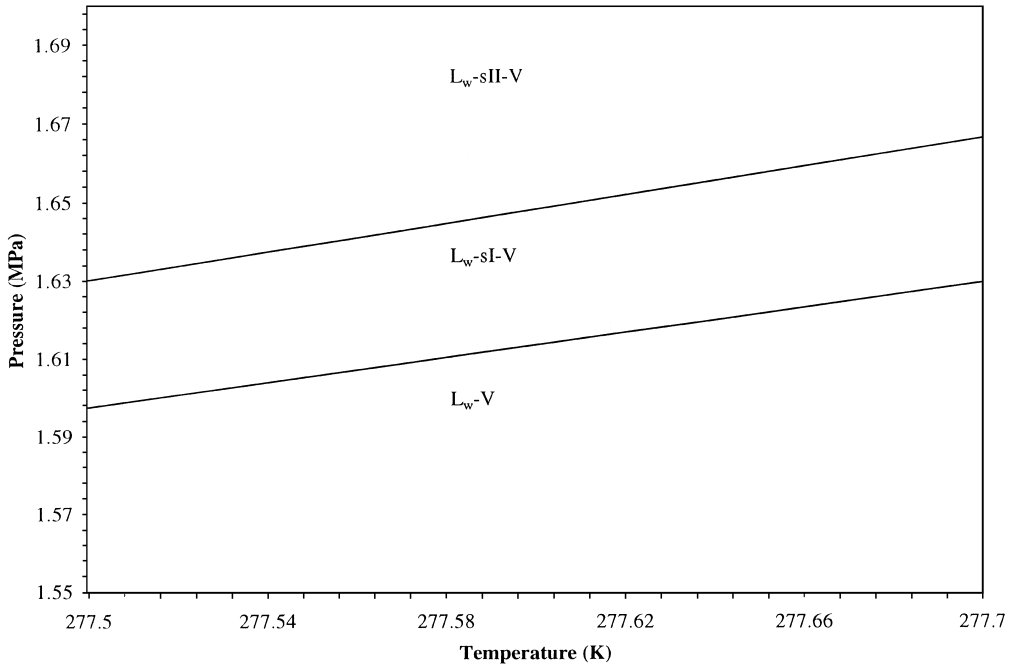

Fig. 5. A section of the pressure versus temperature (P–T) diagram for methane + ethane + water system at $y_{CH_4} = 0.73$. Note that the hydrate structure changes from sI to sII for a small change in pressure of about 0.03 MPa at a given temperature.

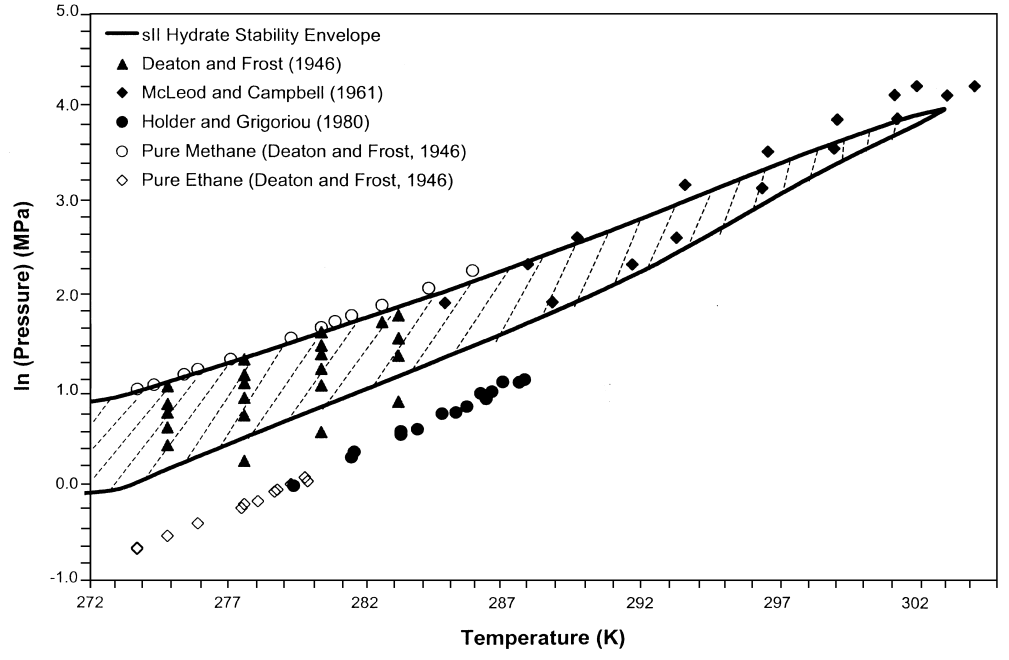

Fig. 6. A semi-log plot of pressure versus temperature that contains the entire incipient hydrate equilibrium literature data set for the methane + ethane + water system. This is overlapped with sII stability envelope, which is the locus of structural transition points in this system.

This work also demonstrates the importance of studying phase behavior above incipient hydrate formation conditions. As shown in Figs. 4 and 5, a small increase in pressure above incipient conditions can either cause a change in the hydrate structure or result in structural coexistence. This might be important in pipeline situations where hydrates typically form at conditions well away from the incipient point. Also in scenarios where kinetic inhibitors are used to impede hydrate growth, the effectiveness of the inhibitor may be jeopardized due to the formation of different or multiple hydrate structures. The dependence of inhibitor effectiveness on hydrate

structure has been demonstrated in the case of polyvinylcaprolactam (PVCap) by Larsen (1997).

The importance of phase behavior above incipient conditions can also be demonstrated by considering stable versus metastable hydrate phases. The pressure versus methane composition (P–x) diagram in Fig. 7 shows the stable sI and sII equilibrium lines (solid lines) and the metastable sI and sII equilibrium lines (dashed lines) for the methane + ethane + water system at 277.6 K. The metastable lines are predicted assuming one of the unstable structures, sI or sII, to be present in the system in place of the stable structure. The closeness in formation pressures of stable sII versus metastable sI in the composition region $0.74 < y_{CH_4} < 0.993$ suggests that researchers working on hydrate formation kinetics need to be aware that a metastable structure can form in conjunction with the stable structure when the system pressure is only slightly above the incipient formation pressure.

In nature, hydrates occur in both oceanic and permafrost environments. In the oceans, the hydrates are mostly methane up to 99% or more. For instance, the gas found close to the hydrates offshore Brazil was mostly methane and the rest (0.1–1%) comprised of ethane and the higher paraffins (Fontana & Mussumeci, 1994). In such cases, the hydrate structure is usually assumed to be sI. But, our results suggest that sII hydrates are stable when as little as 0.7 mol% of ethane is present.

If naturally occurring hydrates are sII, it might directly affect the exact location of the hydrate stability boundary in oceanic and permafrost sediments. The amount of methane trapped in the hydrate will change with a change in structure from sI to sII as demonstrated in this work and our previous work (Subramanian et al., 2000). These two factors can affect calculations concerning the amount of methane trapped in hydrates and hence the potential of naturally occurring hydrates as a future energy resource.

7. Conclusions

This work reports results from Raman and NMR studies on structural transitions in the methane + ethane hydrate system. Raman results indicate that, at 274.2 K, the upper transition point involving a change in structure from sII to sI occurs over the vapor methane mole fraction range of 0.992 ($\pm$ 0.005)–0.994 ($\pm$ 0.007). This indicates that a trace amount of ethane can be sufficient to drive the hydrate structure from sI to sII.

^{13}C NMR spectra used to measure the water-free guest composition of the hydrate phase at various vapor compositions at 253 K suggest that the mole fraction of methane in hydrate increases by about 0.2 with the change in structure from sI to sII at the lower transition point.

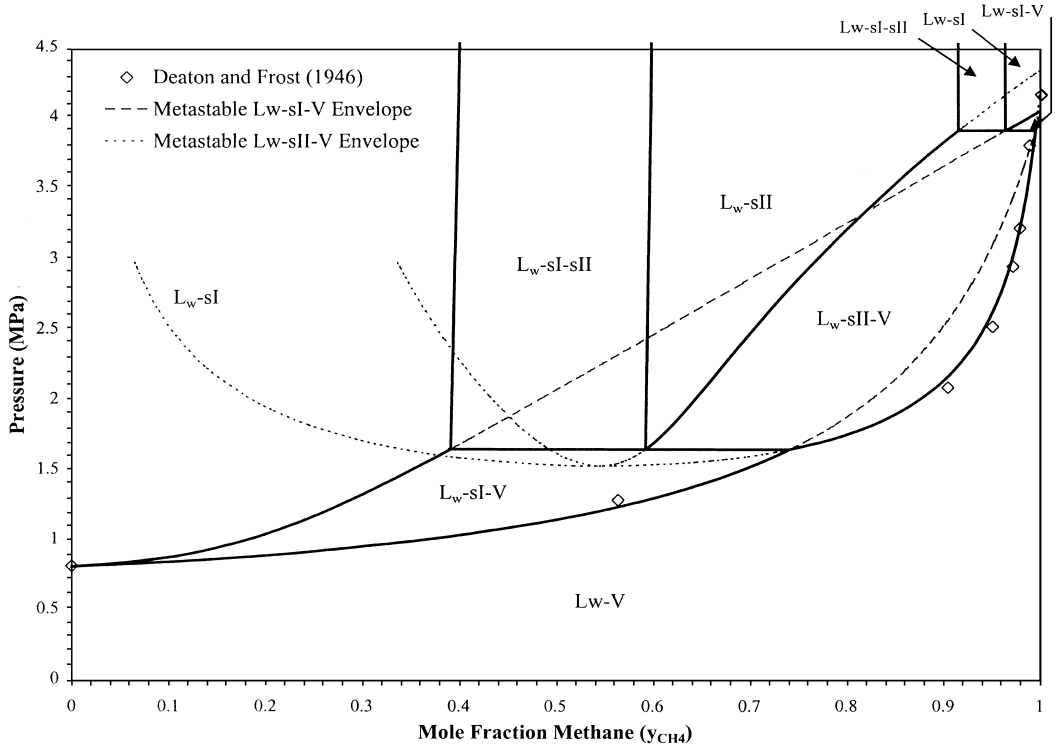

Fig. 7. Pressure–composition diagram for methane + ethane + water at 277.6 K, along with metastable L_w–sI–V and L_w–sII–V envelopes. Note that above $y_{CH_4} = 0.74$, the L_w–H–V equilibrium pressure for sII hydrate is less than that for metastable sI hydrate.

In our modeling efforts, a complete phase diagram for the methane + ethane + water system was generated using a corrected set of Kihara parameters optimized to fit the experimentally determined lower transition point. Regions of this phase diagram indicate changes in hydrate structure and coexistence of multiple structures at pressures above incipient formation conditions. However, these predictions need to be experimentally verified in the future.

Both experimental and modeling results presented here have important implications for future hydrate research. Some of these are better model parameters leading to accurate hydrate predictions for natural gas systems containing methane and ethane, and the possibility of sII hydrate formation in oceanic and permafrost sediments. This study also demonstrates the need to measure the hydrate structure along with phase equilibria experiments to facilitate accurate modeling.

Acknowledgements

The National Science Foundation provided funding for the Raman and NMR part of this work through the Research Grant CTS-9634899. The NMR spectra were obtained in the Colorado School of Mines NMR Facility, which is funded by a NSF award CTS-9512228. A. B. is supported through a consortium of oil companies, viz. ARCO, Chevron, Department of Energy, Mobil, Phillips, Shell and Texaco.

References

Ballard, A.L., & Sloan Jr., E. D. (2000). Optimizing thermodynamic parameters to match methane and ethane structural transition in natural gas hydrate equilibria. *Proceedings of the third international conference on gas hydrates*, Salt Lake City, Utah, July 19–24, 1999, *Annals of the New York Academy of Sciences*, vol. 912 (pp. 702). New York.

Bishnoi, P. R., Gupta, A. K., Englezos, P., & Kalogerakis, N. (1989). Multiphase equilibrium flash calculations for systems containing gas hydrates. *Fluid Phase Equilibria*, *53*, 97–104.

Deaton, W. M., & Frost Jr., E. M. (1946). The U. S. Bureau of Mines, Monograph 8.

Englezos, P., Kalogerakis, N., Dholabhai, P. D., & Bishnoi, P. R. (1987a). Kinetics of formation of methane and ethane gas hydrates. *Chemical Engineering Science*, *42*(11), 2647–2658.

Englezos, P., Kalogerakis, N., Dholabhai, P. D., & Bishnoi, P. R. (1987b). Kinetics of gas hydrate formation from mixtures of methane and ethane. *Chemical Engineering Science*, *42*(11), 2659–2666.

Fontana, R. L., & Mussumeci, A. (1994). Hydrates offshore Brazil. *International conference on natural gas hydrates*, June 20–24, New Paltz, New York, 1993, *Annals of New York Academy of Sciences*, vol. 715, 106.

Gupta, A. K. (1990). *Steady state simulation of chemical processes*. Ph.D. Thesis, University of Calgary, Calgary, Canada.

Gupta, A. K., Bisnoi, P. R., & Kalogerakis, N. (1991). A method for the simultaneous phase equilibria and stability calculations for multiphase reacting and non-reacting systems. *Fluid Phase Equilibria*, *63*, 65–89.

Holder, G. D., & Grigoriou, G. C. (1980). Hydrate dissociation pressures of (methane + ethane + water), Existence of a locus of minimum pressures. *Journal of Chemical Thermodynamics*, *12*, 1093–1104.

Holder, G. D., & Hand, J. H. (1982). Multiple-phase equilibria in hydrates from methane, ethane, propane, and water mixtures. *A.I.Ch.E. Journal*, *28*, 440–447.

Katz, D.L., Cornell, D., Vary, J.A., Kobayashi, R., Elenbaas, J.R., Poettmann, F.H., & Weinaug, C.F. (1959). *Handbook of natural gas engineering*. New York: McGraw-Hill, Book Company, Inc.

Larsen, R. (1997). *Clathrate hydrate single crystals: Growth and inhibition*. D. Ing. thesis, Norwegian University of Science and Technology.

McLeod, H. O., & Campbell, J. M. (1961). Natural gas hydrates at pressures to 10,000 psia. *Journal of Petroleum Technology*, *222*, 590–594.

Miyoshi, T., Takegoshi, K., & Terao, T. (1997). A simple method for ^{13}C CP MAS NMR experiments under high gas pressures. *Journal of Magnetic Resonance*, *125*, 383.

Parrish, W. R., & Prausnitz, J. M. (1972). Dissociation pressures of gas hydrates formed by gas mixtures. *Industrial and Engineering Chemical Process Design and Development*, *11*(1), 26.

Skovborg, P., & Rasmussen, P. (1994). A mass transport limited model for the growth of methane and ethane gas hydrates. *Chemical Engineering Science*, *49*(8), 1131–1143.

Sloan, E. D. (1998). *Clathrate hydrates of natural gases* (2nd ed.) (p. 705 and software). New York: Marcel Dekker Inc.

Stackelberg, M. von, & Jahns, W. (1954). Feste gashydrate VI: Die gitteraufweitungsarbeit. *Zeitschrift fuer Elektrochemie, 58*, 162–164.

Subramanian, S., Kini, R. A., Dec, S. F., & Sloan, E. D. (2000). Evidence of structure II hydrate formation from methane + ethane mixtures. *Chemical Engineering Science*, *55*(11), 1981–1999.

Sum, A. K., Burruss, R. C., & Sloan, E. D. (1997). Measurement of clathrate hydrates via Raman spectroscopy. *Journal of Physical Chemistry B*, *101*, 7371.

van Geet, A. L. (1970). Calibration of nuclear magnetic resonance thermometer at low temperatures. *Analytical Chemistry*, 42, 679–680.

van der Waals, J. H., & Platteeuw, J. C. (1959). Clathrate solutions. *Advanced Chemical Physics, 2*, 1–57.